Reduced Subthreshold Characteristics and Flicker Noise of an AlGaAs/InGaAs PHEMT Using Liquid Phase Deposited TiO$_2$ as a Gate Dielectric

Kai-Yuen Lam [1], Jung-Sheng Huang [1], Yong-Jie Zou [1], Kuan-Wei Lee [1,*] and Yeong-Her Wang [2]

[1] Department of Electronic Engineering, I-Shou University, Kaohsiung 840, Taiwan;
kylam@isu.edu.tw (K.-Y.L.); jshuang@isu.edu.tw (J.-S.H.); gp30083@msn.com (Y.-J.Z.)

[2] Department of Electrical Engineering, Institute of Microelectronics, National Cheng-Kung University,
Tainan 701, Taiwan; yhw@ee.ncku.edu.tw

* Correspondence: kwlee@isu.edu.tw; Tel.: +886-7-6577711 (ext. 6679)

Abstract: This study presents the fabrication and improved properties of an AlGaAs/InGaAs metal-oxide-semiconductor pseudomorphic high-electron-mobility transistor (MOS-PHEMT) using liquid phase deposited titanium dioxide (LPD-TiO$_2$) as a gate dielectric. Sulfur pretreatment and postoxidation rapid thermal annealing (RTA) were consecutively employed before and after the gate dielectric was deposited to fill dangling bonds and therefore release interface trapped charges. Compared with a benchmark PHEMT, the AlGaAs/InGaAs MOS-PHEMT using LPD-TiO$_2$ exhibited larger gate bias operation, higher breakdown voltage, suppressed subthreshold characteristics, and reduced flicker noise. As a result, the device with proposed process and using LPD-TiO$_2$ as a gate dielectric is promising for high-speed applications that demand little noise at low frequencies.

1. Introduction

The performances of GaAs-based pseudomorphic high-electron-mobility transistors (PHEMTs) have drastically been improved, and have already been extensively used in both low-noise and high-power applications at microwave and millimeter-wave frequencies [1–4]. However, microwave device manufacturing is still being challenged to achieve high uniformity, high yield, and reliable stability. Hartnagel et al. [5] and Huang et al. [6] describe that major noises in PHEMTs contain thermal noise, shot noise, hot-electron noise, and generation-recombination noise. Shot noise related to the Schottky barrier affects the gate leakage current, and plays an important role in low-noise applications. Hot-electron noise, caused by energetic random electron motion, is associated with impact ionization. Electrons gain energy from supplied electric field and can be randomized by optical phonons, intervalley scattering. If electrons gain enough energy, they can collide with electron–hole pair or impurity and start ionization process. Impact ionization creates current fluctuations and thus is one of the strongest electronic noise sources. Generation-recombination noise induced by the surface recombination centers or defects at the gate terminal/Schottky layer interface can increase the ideality factor, and also produce traps that can contribute to flicker noise. Thus, the Schottky-gate PHEMTs have limited gate leakage current and noise performance levels.

High-κ materials are widely employed as insulators growing on semiconductor to fabricate metal-oxide-semiconductor (MOS) gates for larger gate swing voltages and lower leakage currents [7–9]. Titanium dioxide (TiO$_2$) is one of the commonly applied high-κ insulators in the semiconductor industry. Numerous methods have been used to successfully deposit TiO$_2$ films, such as low-pressure

chemical vapor deposition (LPCVD) [10], plasma-enhanced chemical vapor deposition (PECVD) [11], sputtering [12], electron beam evaporation [13], sol-gel deposition [14], and liquid phase deposition (LPD) [15]. Among those methods, LPD is favorable for its low-cost and low-temperature process. LPD-TiO_2 films have respectively been demonstrated on InP [16], polysilicon [17], glass [18], GaN [19], and AlGaAs [20]. We also previously conducted a preliminary study of LPD-TiO_2 on AlGaAs without pretreatment [20], and made the LPD-TiO_2 more compact through sulfide pretreatment [21] and postoxidation rapid thermal annealing (RTA) [22]. However, the low-frequency noise and microwave characteristics of AlGaAs/InGaAs MOS-PHEMT prepared with both ammonium-sulfide-pretreated AlGaAs and postoxidation RTA have not been investigated yet. In this study, an AlGaAs/InGaAs MOS-PHEMT using LPD-TiO_2 as a gate dielectric after sulfide pretreatment and postoxidation RTA was fabricated, and dc characteristics and microwave performance were discussed.

2. Experimental

The proposed device structures were grown through metal-organic chemical vapor deposition on a semi-insulating GaAs substrate. The buffer layer consisted of a 100 nm layer of *i*-GaAs, followed by a 250 nm layer of *i*-$Al_{0.2}Ga_{0.8}As$, and a 60 nm layer of GaAs. A 10 nm layer of $Al_{0.2}Ga_{0.8}As$ with a Si doping density of 4.5×10^{17} cm^{-3} and a 2 nm *i*-$Al_{0.2}Ga_{0.8}As$ spacer layer were then grown on the buffer layer, followed by a 14 nm *i*-$In_{0.15}Ga_{0.85}As$ channel layer, a 2 nm *i*-$Al_{0.2}Ga_{0.8}As$ spacer layer, a 18 nm $Al_{0.2}Ga_{0.8}As$ donor layer with a Si doping density of 1.2×10^{18} cm^{-3}, a 70 nm $Al_{0.2}Ga_{0.8}As$ Schottky layer with a Si doping density of 1×10^{17} cm^{-3}, and a 60 nm GaAs cap layer with a Si doping density of 5×10^{18} cm^{-3}. Hall measurements showed that the electron mobility was 5900 cm^2/V·s and the electron sheet density was 2.1×10^{12} cm^{-2} at 300 K.

Wafers were first cleaned using acetone, methanol, and H_2O for 5 min with each solvent. A NH_4OH:H_2O_2:H_2O (=3:1:50 by volume) solution was used to perform mesa etching, which reached the GaAs buffer layer. Ohmic contacts composed of a 400 nm layer of Au/Ge/Ni alloy (84:12:4 by weight) were deposited through evaporation and then patterned through lift-off processes, followed by RTA at 380 °C for 30 s. After the cap layer and part of the Schottky layer had been etched using the same etchant, the wafer was immediately dipped into a 5% $(NH_4)_2S_x$ solution for 10 min. For the referenced PHEMT, Au was deposited directly on the sulfide-treated AlGaAs of the Schottky layer. For the MOS-PHEMT, following the $(NH_4)_2S_x$ pretreatment, the LPD-TiO_2 was applied on the sulfide-treated Schottky layer at 40 °C [19]. Oxide thickness was approximately 30 nm after postoxidation RTA at 350 °C for 1 min. Finally, the gate electrode was formed through lift-off with Au on the oxide layer. Figure 1 shows the structures of the referenced PHEMT and MOS-PHEMT. The gate length, gate width, and the drain-to-source spacing are 1 μm, 100 μm, and 5 μm, respectively. In addition, the oxide passivated the etched isolated surface wall simultaneously. Microwave on-wafer measurements were conducted from 0.45 to 50 GHz in a common-source configuration by using an Agilent E8364A PNA network analyzer at 300 K.
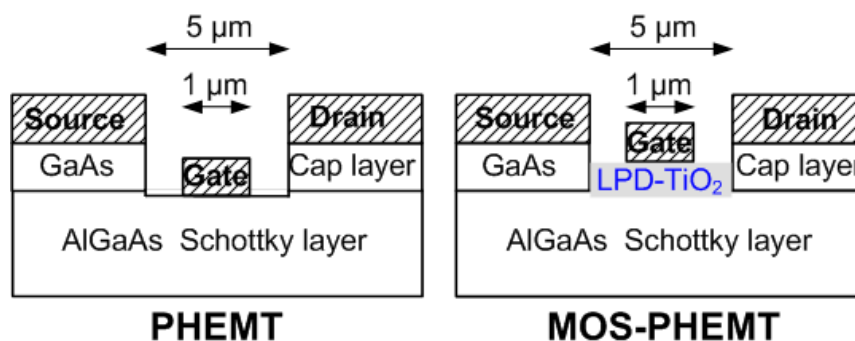

Figure 1. Schematic structures of AlGaAs/InGaAs PHEMT and MOS-PHEMT.

3. Results and Discussion

Figure 2a shows the X-ray diffraction (XRD) patterns of the LPD-TiO$_2$ that was deposited on the sulfide-pretreated AlGaAs with and without postoxidation RTA for 1 min. The XRD patterns did not show peaks corresponding to the anatase or rutile phases when the annealing temperature was raised to 400 °C. The results indicate that the LPD-TiO$_2$ lacked sufficient energy to form a single phase or a polycrystal phase at temperatures no greater than 400 °C during the annealing process. Figure 2b shows the 1 MHz capacitance-voltage (C-V) characteristics of the referenced PHEMT and the MOS-PHEMT. The capacitance of the MOS-PHEMT was lower than that of the PHEMT, because the LPD-TiO$_2$ was in series with the PHEMT. The relative dielectric constant (ε_r) of the LPD-TiO$_2$ can be calculated using the following equation:

$$C_{OX} = \frac{\varepsilon_r \cdot \varepsilon_0 \cdot A}{t_{OX}} \tag{1}$$

where C$_{OX}$ is the capacitance of the LPD-TiO$_2$, ε_0 is the permittivity of free space, A is the metal plate area, and t_{OX} is the oxide thickness. The calculated ε_r of the LPD-TiO$_2$ was approximately 21, fitting the range of amorphous TiO$_2$, which was comparable to the ε_r value (24.4) for GaN using the same method [19] and to the ε_r value for polysilicon found by other group [17].
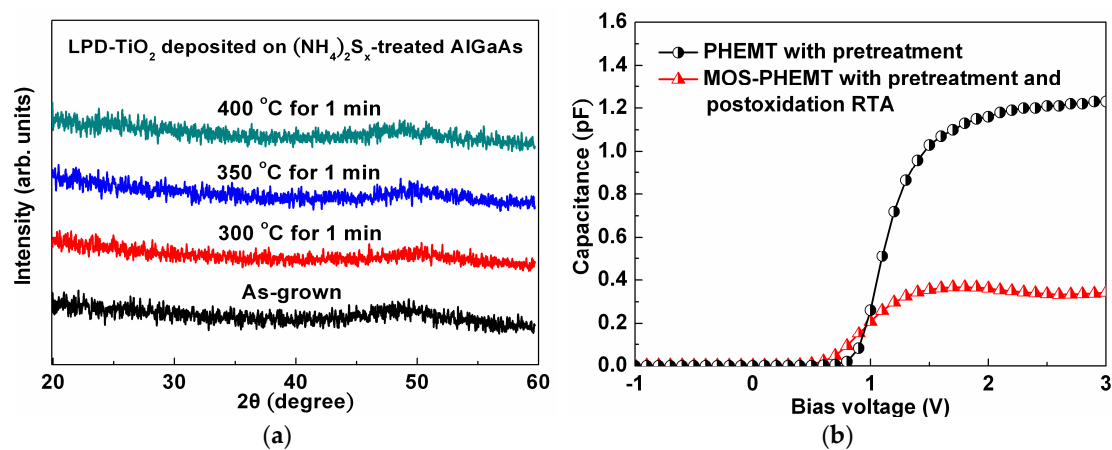

Figure 2. (**a**) XRD spectra of LPD-TiO$_2$ deposited on sulfide-pretreated AlGaAs with and without postoxidation RTA; (**b**) C-V comparison for sulfide-pretreated PHEMT and MOS-PHEMT with postoxidation RTA.

Figure 3a,b shows the transconductance (g$_m$) and the drain current density (I$_D$) as functions of the gate-to-source voltage (V$_{GS}$) at a drain-to-source voltage (V$_{DS}$) = 2 V. The maximum g$_m$ values were 170 mS/mm and 132 mS/mm for the referenced PHEMT and the MOS-PHEMT, respectively. However, the gate voltage swing (defined by a 10% reduction of the maximal g$_m$) was 0.8 V for the MOS-PHEMT, which was higher than that of referenced case. The insets show the related I$_D$-V$_{DS}$ characteristics for both devices. The maximal V$_{GS}$ of the MOS-PHEMT was larger than that of the referenced PHEMT because the MOS-PHEMT had a higher energy barrier between the metal gate and AlGaAs Schottky layer. The maximal I$_D$ was approximately 270 mA/mm at V$_{GS}$ = 0.5 V and V$_{DS}$ = 2 V for PHEMT. However, the maximal I$_D$ was approximately 200 mA/mm at V$_{GS}$ = 0.5 V and V$_{DS}$ = 2 V, and 420 mA/mm at V$_{GS}$ = 4 V and V$_{DS}$ = 6 V for MOS-PHEMT. The MOS-PHEMT saturation current was less than that of the referenced case at the same V$_{GS}$ because of the voltage drop of the LPD-TiO$_2$ underneath the metal gate. However, it was able to induce carriers V$_{GS}$ from 0.5 to 4 V within the channel. By the way, the notable difference of the threshold voltages (V$_{th}$) between capacitor and PHEMT is owing to the different depth of gate recess by wet etchant from different batches.
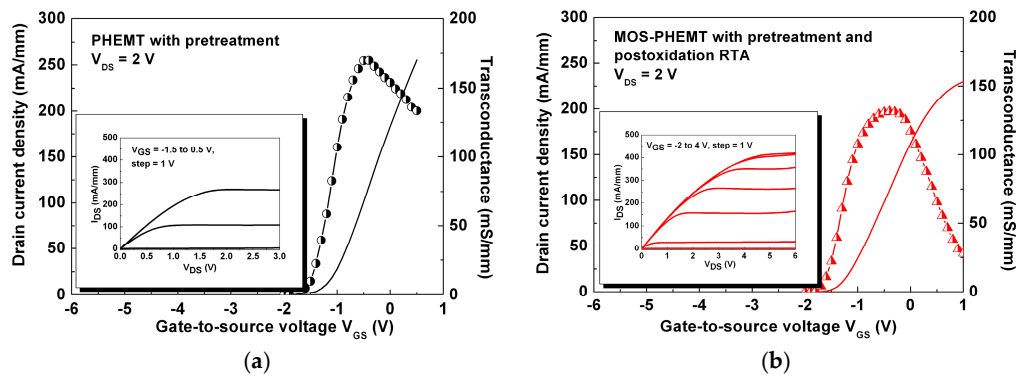
Figure 3. (**a**) Measured I–V characteristics and related transconductance curves for referenced PHEMT; (**b**) Measured I–V characteristics and related transconductance curves for MOS-PHEMT.

The subthreshold characteristics depend on the quality of oxide film and device structure. They determine the ideal off state, and they have effects on power dissipation and IC applications. Figure 4a,b shows the measured subthreshold currents of the referenced PHEMT and MOS-PHEMT, respectively. The subthreshold swing (SS) of the MOS-PHEMT (120 to 125 mV/dec) was lower than that (173 to 194 mV/dec) of the referenced PHEMT. The I_{ON}/I_{OFF} ratio of the MOS-PHEMT (8.1×10^3 to 4.1×10^4) was higher than that (4.8×10^3 to 1.5×10^4) of the referenced case, where I_{ON} was I_D at $V_{GS} = V_{th} + 0.5$ V, and I_{OFF} was I_D at $V_{GS} = V_{th} - 1$ V. These results clearly suggest that the MOS-PHEMT suppressed its subthreshold current by reducing the surface recombination current of the LPD-TiO_2 around the ohmic contact region. That is, the undesirable carrier injection from the source terminal in an off state can be suppressed. Improvements of the SS and I_{ON}/I_{OFF} ratio were also associated with suppressed gate leakage characteristics [23], and this association is consistent with the results shown in Figure 5.
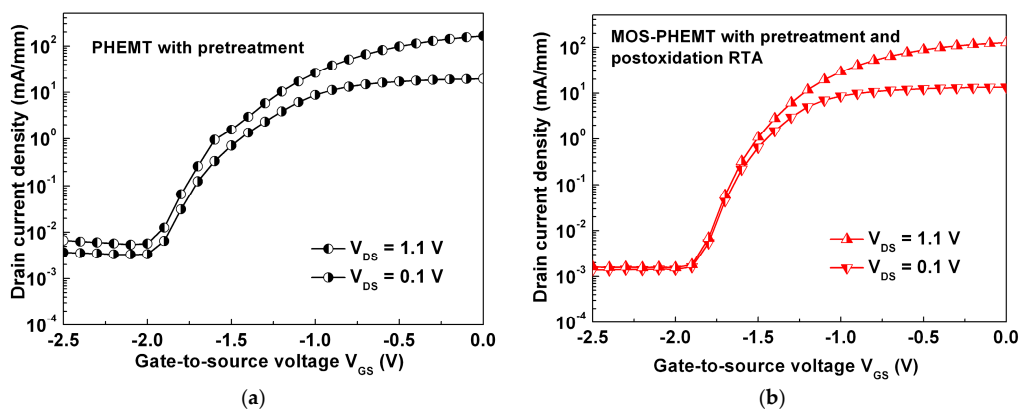

Figure 4. Subthreshold characteristics of: (**a**) referenced PHEMT; and (**b**) MOS-PHEMT with $V_{DS} = 0.1$ V and 1.1 V.

The LPD-TiO_2 caused an improvement in the breakdown voltage associated with the gate leakage current of the typical gate-to-drain diode characteristics, as shown in Figure 5. Figure 5a shows that the turn-on voltage (V_{on}) of the MOS-PHEMT, 1.5 V, was obviously higher than that of the referenced PHEMT, 1.1 V. For the MOS-PHEMT, the gate leakage current density was suppressed by approximately two orders of magnitude, and the corresponding reverse gate-to-drain breakdown voltage (BV_{GD}) was more than -21.2 V, as shown in Figure 5b. The V_{on} and the BV_{GD} were defined as the voltage at which the gate current reaches 1 mA/mm. Generally, an increased V_{on} accompanies an improved gate voltage swing. The gate leakage current density of the MOS-PHEMT was lower because of the MOS structure and the elimination of the sidewall leakage path passivated by the LPD-TiO_2.
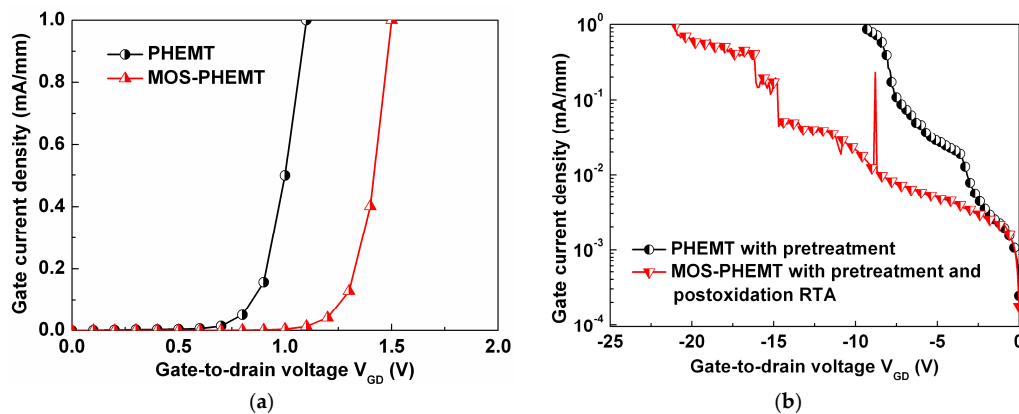
Figure 5. (**a**) Forward gate leakage current density; and (**b**) magnified section of reverse gate leakage current density of typical gate-to-drain diode characteristics for both devices.

The gate current density, as a function of V_{GS}, was measured to obtain insights on the influence of impact ionization. Because of the deep-complex (DX)-center and surface states of AlGaAs, the impact ionization or kink effect is key concern for the AlGaAs/InGaAs PHEMT. A roughly bell-shaped curve is the typical behavior of impact ionization, as shown in Figure 6a for the PHEMT. Marked increases in the gate current clearly occur when devices are biased at higher V_{DS}. The gate current densities of the MOS-PHEMT and PHEMT were 4.59×10^{-3} mA/mm and 2.47×10^{-2} mA/mm at $V_{DS} = 5$ V and $V_{GS} = -4$ V, as shown in Figure 6a,b, respectively; therefore the MOS-PHEMT device's performance was approximately 5.4 times higher than that of the PHEMT. In the referenced PHEMT, significant hot-electron phenomena occurred in the InGaAs channel because of a high electric field near the gate-to-drain region; that is, electrons could obtain higher energy to generate electron–hole pairs through enhanced impact ionizations in the InGaAs channel, which facilitated injection of the holes into the gate terminal [24] or becoming trapped in pre-existing traps. Furthermore, the generation of holes by impact ionization and their further recombination could result in fluctuations of the charges pileup and thus the excess noise. These phenomena also led to increased high-frequency noise at corresponding voltages [25]. In the MOS-PHEMT, the electric field near the gate-to-drain region at the same V_{DS} and V_{GS} improved notably compared with the values of the referenced case, because of the high barrier height of LPD-TiO$_2$ underneath the gate terminal. Thus, the improvements of the MOS-PHEMT resulted in a smaller channel electric field and a suppressed impact ionization that further reduced the leakage current density. As mentioned earlier, the suppressed leakage current and impact ionization effect in Figure 6b were expected to improve noise performance.
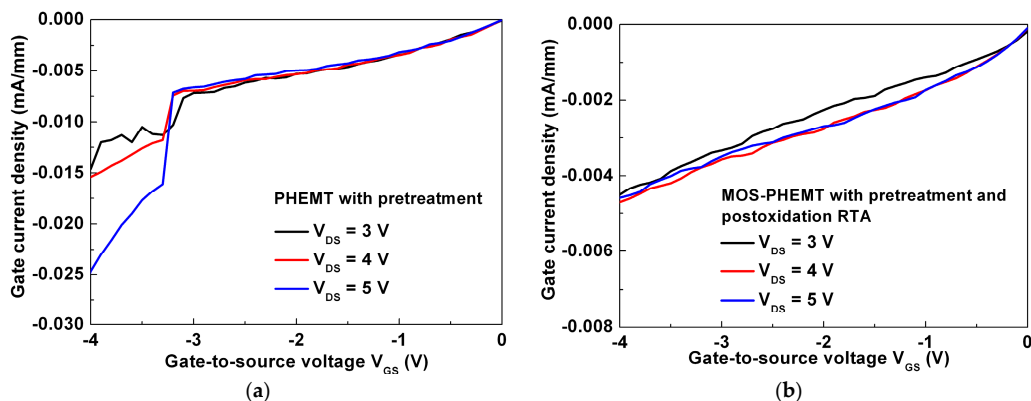

Figure 6. Gate current density versus V_{GS} with different V_{DS} for: (**a**) referenced PHEMT; and (**b**) MOS-PHEMT.

As shown in Figure 7 (different samples from those shown in Figure 3), the measured unity-current-gain cutoff frequency (f_T) and the maximum oscillation frequency (f_{max}) were 17.3 (11.6) GHz and 26.4 (19.7) GHz at the maximum g_m for the MOS-PHEMT (PHEMT). The trend is consistent with the results previously found for E-mode InGaP/InGaAs MOS-PHEMT with liquid phase oxidation (LPO) [26]. The increased microwave performances of the AlGaAs/InGaAs MOS-PHEMT may be attributed to the increase in the ratio of g_m to gate-source capacitance (C_{gs}). Furthermore, the reduction of the surface recombination may also have contributed to the frequency response.
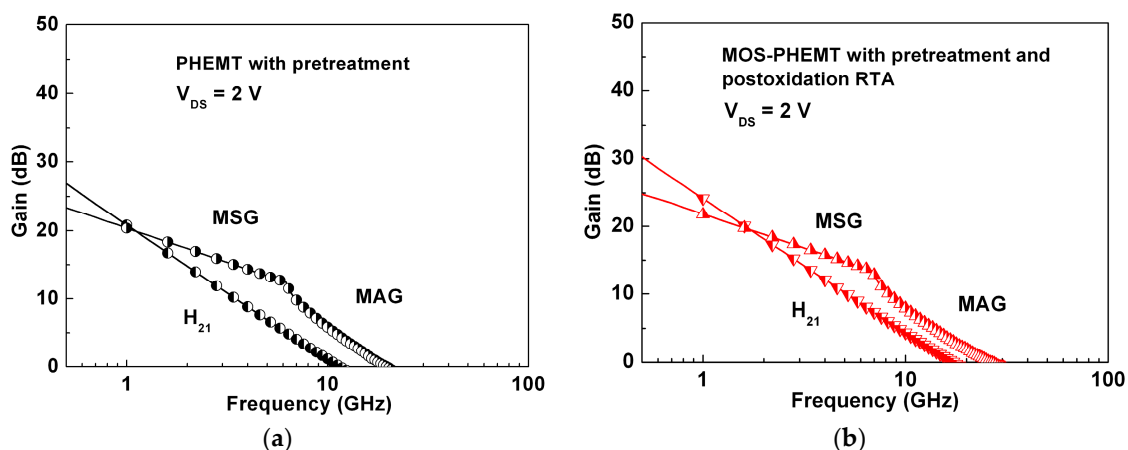

Figure 7. Comparison of microwave characteristics at maximum g_m for: (**a**) referenced PHEMT; and (**b**) MOS-PHEMT.

Figure 8 shows the low-frequency flicker noise spectral density (S_V) characteristics, which were measured using a BTA 9812B noise analyzer and an Agilent 35670A dynamic signal analyzer. On-wafer flicker noise measurements of the referenced AlGaAs/InGaAs PHEMT and AlGaAs/InGaAs MOS-PHEMT were conducted under V_{DS} of 2 V and drain current of 3 mA for frequencies between 10 Hz and 100 kHz. S_V can be expressed as follows [27]:

$$S_V = \left(\frac{q \cdot \alpha_H \cdot v_{sat}}{f^{\gamma} \cdot L_g} \right) \cdot \left(\frac{I_{D,sat}}{g_m^2} \right) \qquad (2)$$

where q is the elementary charge, α_H is the Hooge parameter, v_{sat} is the effective carrier saturation velocity, f is the frequency, γ is the frequency exponent, and L_g is the effective gate length. The α_H / S_V values at 10 Hz for the referenced case and MOS-PHEMT were $2.8 \times 10^{-4} / 3.4 \times 10^{-15}$ V$^2 \cdot$Hz^{-1} and $2.7 \times 10^{-5} / 1.4 \times 10^{-15}$ V$^2 \cdot$Hz^{-1}, respectively. The corresponding γ values were calculated to be 1.5 and 1.1, respectively. The higher γ was notably related to generation-recombination noise (i.e., $\gamma = 2$). In other words, the LPD-TiO$_2$ could passivate dangling bonds to improve the surface state between the LPD-TiO$_2$/AlGaAs interfaces, and a reduction of the surface state was observed with negligible low-frequency generation-recombination noise of the AlGaAs/InGaAs MOS-PHEMT.

Table 1 summarizes the dc, low-frequency noise, and microwave characteristics for LPD in this study and previous studies [28,29] and for LPO [30] in AlGaAs/InGaAs MOS-PHEMTs with similar structures but different types of gate oxides. The use of high-*K* LPD-TiO$_2$ with both sulfide pretreatment and postoxidation RTA as a gate oxide and as an effective passivation layer on AlGaAs/InGaAs PHEMT provides new opportunities for low-noise applications.
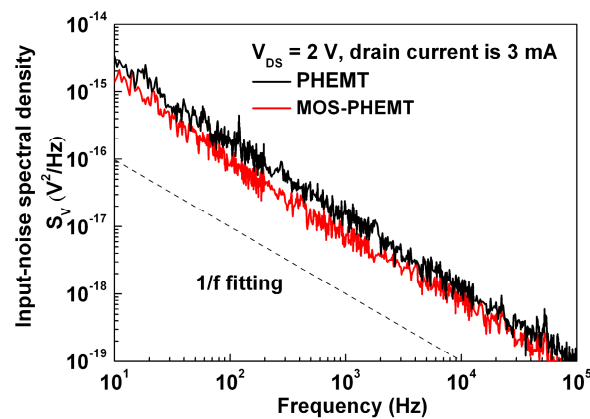
Figure 8. Comparison of low-frequency 1/f characteristics for both devices.

Table 1. Summary of dc, low-frequency noise, and microwave characteristics of AlGaAs/InGaAs MOS-PHEMTs with similar structures but different types of gate oxides.

Group	This Work	[28]	[29]	[30]
Mode	D-mode	D-mode	D-mode	D-mode
Gate oxide	TiO_2	SiO_2	Al_2O_3	Oxidized AlGaAs
Oxidation method	LPD	LPD	LPD	LPO
Temperature ($°C$)	40	40	40	50
Gate length (μm)	1	1	1	1
Maximum V_{GS} (V)	4	4	2.5	4
Maximum I_{DS} (mA/mm)	420	421	433	380
Gate voltage swing (V)	0.8	2.5	2	0.7
SubthresholdSwing (mV/dec)	120–125	125–165	–	–
S_V at 10 Hz ($V^2 \cdot Hz^{-1}$)	1.4×10^{-15}	–	–	–
f_{max} (GHz)	26.4	–	–	–

4. Conclusions

This study demonstrates the feasibility of preparing an LPD-TiO_2 gate with both sulfide pretreatment and postoxidation RTA on AlGaAs/InGaAs MOS-PHEMT near room temperature. Compared with the referenced PHEMT, the MOS-PHEMT had larger gate voltage swing, lower subthreshold characteristics, reduced gate leakage current (with a suppressed impact ionization), enhanced microwave performance, and reduced flicker noise. These features evidence that the proposed device with simple and low-temperature LPD-TiO_2 gate is suitable for device applications.

Author Contributions: Kuan-Wei Lee conceived and designed the experiments; Yong-Jie Zou performed the experiments; Kuan-Wei Lee and Jung-Sheng Huang analyzed the data; Yeong-Her Wang contributed materials and analysis tools; Kai-Yuen Lam wrote the paper.

Conflicts of Interest: The authors declare no conflict of interest.

References

1.   Lee, H.L.; Moon, S.M.; Dong, H.J.; Lee, M.Q.; Yu, J.W. K-band 0/180° Balanced Phase Shifter with DC-Offset Cancellation. *Electron. Lett.* **2013**, *49*, 1234–1235. [CrossRef]
2.   Lin, Y.S.; Wu, J.F.; Hsia, W.F.; Wang, P.C.; Chung, Y.H. Design of Electronically Switchable Single-to-Balanced Bandpass Low-Noise Amplifier. *IET Microw. Antennas Propag.* **2013**, *7*, 510–517. [CrossRef]

3. Nikandish, G.; Babakrpur, E.; Medi, A.A. Harmonic Termination Technique for Single- and Multi-Band High-Efficiency Class-F MMIC Power Amplifiers. *IEEE Trans. Microw. Theory Tech.* **2014**, *62*, 1212–1220. [CrossRef]

4. Ding, X.; Zhang, L. A High-Efficiency GaAs MMIC Power Amplifier for Multi-Standard System. *IEEE Microw. Wirel. Compon. Lett.* **2016**, *26*, 55–57. [CrossRef]

5. Hartnagel, H.; Katilius, R.; Matulionis, A. *Microwave Noise in Semiconductor Devices*; John Wiley & Sons, Inc.: Hoboken, NJ, USA, 2001.

6. Huang, H.K.; Wang, C.S.; Chang, C.P.; Wang, Y.H.; Wu, C.L.; Chang, C.S. Noise Characteristics of InGaP-gated PHEMTs under High Current and Thermal Accelerated Stresses. *IEEE Trans. Electron. Devices* **2005**, *52*, 1706–1712. [CrossRef]

7. Yagi, S.; Shimizu, M.; Inaga, M.; Yamamoto, Y.; Piao, G.; Okumura, H.; Yano, Y.; Akutsu, N.; Ohashi, H. High Breakdown Voltage AlGaN/GaN MIS-HEMT with SiN and TiO_2 Gate Insulator. *Solid State Electron.* **2006**, *50*, 1057–1061. [CrossRef]

8. Hu, C.C.; Lin, M.S.; Wu, T.Y.; Adriyanto, F.; Sze, P.W.; Wu, C.L.; Wang, Y.H. AlGaN/GaN Metal-Oxide-Semiconductor High-Electron Mobility Transistor with Liquid-Phase-Deposited Barium-Doped TiO_2 as a Gate Dielectric. *IEEE Trans. Electron. Devices* **2012**, *59*, 121–127. [CrossRef]

9. Choi, W.; Seok, O.; Ryu, H.; Cha, H.Y.; Seo, K.S. High-Voltage and Low-Leakage-Current Gate Recessed Normally-Off GaN MIS-HEMTs with Dual Gate Insulator Employing PEALD-SiN_x/RF-Sputtered-HfO_2. *IEEE Electron. Device Lett.* **2014**, *35*, 175–177. [CrossRef]

10. Yokozawa, M.; Iwasa, H.; Teramoto, I. Vapor Deposition of TiO_2. *Jpn. J. Appl. Phys.* **1967**, *7*, 96–97. [CrossRef]

11. Ha, H.K.; Yoshimoto, M.; Koinuma, H.; Moon, B.K.; Ishiwara, H. Open Air Plasma Chemical Vapor Deposition of Highly Dielectric Amorphous TiO_2 Films. *Appl. Phys. Lett.* **1996**, *68*, 2965–2967. [CrossRef]

12. Martin, N.; Rousselot, C.; Savall, C.; Palmino, F. Characterizations of Titanium Oxide Films Prepared by Radio Frequency Magnetron Sputtering. *Thin Solid Films* **1996**, *287*, 154–163. [CrossRef]

13. Yang, T.S.; Shiu, C.B.; Wong, M.S. Structure and Hydrophilicity of Titanium Oxide Films Prepared by Electron Beam Evaporation. *Surf. Sci.* **2004**, *548*, 75–82. [CrossRef]

14. Sonawane, R.S.; Hegde, S.G.; Dongare, M.K. Preparation of Titanium (IV) Oxide Thin Film Photocatalyst by Sol-Gel Dip Coating. *Mater. Chem. Phys.* **2003**, *77*, 744–750. [CrossRef]

15. Wang, X.P.; Yu, Y.; Hu, X.F.; Gao, L. Hydrophilicity of TiO_2 Films Prepared by Liquid Phase Deposition. *Thin Solid Films* **2000**, *371*, 148–152. [CrossRef]

16. Lee, M.K.; Huang, J.J.; Shih, C.M.; Cheng, C.C. Properties of TiO_2 Thin Films on InP Substrate Prepared by Liquid Phase Deposition. *Jpn. J. Appl. Phys.* **2002**, *41*, 4689–4690. [CrossRef]

17. Lee, M.K.; Lee, H.C.; Hsu, C.M. High Dielectric Constant TiO_2 Film Grown on Polysilicon by Liquid Phase deposition. *Mater. Sci. Semicond. Process.* **2007**, *10*, 61–67. [CrossRef]

18. Mallak, M.; Bockmeyer, M.; Löbmann, P. Liquid Phase Deposition of TiO_2 on Glass: Systematic Comparison to Films Prepared by Sol-Gel Processing. *Solid State Electron.* **2007**, *515*, 8072–8077. [CrossRef]

19. Wu, T.Y.; Lin, S.K.; Sze, P.W.; Huang, J.J.; Chien, W.C.; Hu, C.C.; Tsai, M.J.; Wang, Y.H. AlGaN/GaN MOSHEMTs with Liquid-Phase-Deposited TiO_2 as Gate Dielectric. *IEEE Trans. Electron. Devices* **2009**, *56*, 2911–2916. [CrossRef]

20. Lee, K.W.; Huang, J.S.; Lu, Y.L.; Lee, F.M.; Lin, H.C.; Wu, T.Y.; Wang, Y.H. Investigation of TiO_2 on AlGaAs Prepared by Liquid Phase Deposition and Its Application. *Solid State Electron.* **2011**, *68*, 85–89. [CrossRef]

21. Huang, J.S.; Lee, T.L.; Zou, Y.J.; Lee, K.W.; Wang, Y.H. Sulfide Pretreatment Effects of Liquid Phase deposited TiO_2 on AlGaAs and Its Application. *Vacuum* **2015**, *118*, 100–103. [CrossRef]

22. Hu, C.C.; Lee, T.L.; Zou, Y.J.; Lee, K.W.; Wang, Y.H. Postoxidation Thermal Annealing Effects of Liquid Phase Deposited TiO_2 on $(NH_4)_2S_x$-treated AlGaAs. *Thin Solid Films* **2014**, *563*, 40–43. [CrossRef]

23. Chung, J.W.; Roberts, J.C.; Piner, E.L.; Palacios, T. Effect of Gate Leakage in the Subthreshold Characteristics of AlGaN/GaN HEMTs. *IEEE Electron. Device Lett.* **2008**, *29*, 1196–1198. [CrossRef]

24. Suemitsu, T.; Enoki, T.; Sano, N.; Tomizawa, M.; Ishii, Y. An Analysis of the Kink Phenomena in InAlAs/InGaAs HEMT's Using Two-Dimensional Device Simulation. *IEEE Trans. Electron. Devices* **1998**, *45*, 2390–2399. [CrossRef]

25. Wang, H.; Liu, Y.; Zeng, R.; Tan, C.L. Understanding of the Excess Channel Noise in InAlAs/InGaAs/InPHigh Electron Mobility Transistors in Impact Ionization Regime. *Appl. Phys. Lett.* **2007**, *90*, 103503. [CrossRef]

26. Lee, K.W.; Chen, W.S. Improved Low-Frequency Noise and Microwave Performance of Enhancement-Mode InGaP/InGaAs PHEMT with a Liquid-Phase Oxidized GaAs without a Gate Recess. *ECS Solid State Lett.* **2012**, *2*, Q9–Q11. [CrossRef]

27. Hughes, B.; Fernandez, N.G.; Gladstone, J.M. GaAs FET's with a Flicker-Noise Corner below 1 MHz. *IEEE Trans. Electron. Devices* **1987**, *34*, 733–741. [CrossRef]

28. Lee, K.W. Improved Impact Ionization in AlGaAs/InGaAs PHEMT with a Liquid Phase Deposited SiO_2 as the Gate Dielectric. *ECS J. Solid State Sci. Technol.* **2012**, *2*, Q27–Q29. [CrossRef]

29. Basu, S.; Singh, P.K.; Sze, P.W.; Wang, Y.H. AlGaAs/InGaAs Metal-Oxide-Semiconductor Pseudomorphic High-Electron-Mobility Transistor with Low Temperature Liquid Phase Deposited Al_2O_3 Gate Insulator. *J. Appl. Phys.* **2008**, *104*, 054116. [CrossRef]

30. Lee, K.W.; Sze, P.W.; Wang, Y.H.; Houng, M.P. AlGaAs/InGaAs Metal-Oxide-Semiconductor Pseudomorphic High-Electron-Mobility Transistor with a Liquid Phase Oxidized AlGaAs as Gate Dielectric. *Solid State Electron.* **2005**, *49*, 213–217. [CrossRef]